

Article

Tribofilm Formation and Friction Reduction Performance on Laser-Textured Surface with Micro-Grooved Structures

Qianru Li ¹, Renguo Lu ^{2,*} , Hiroshi Tani ², Shohei Kawada ² , Shinji Koganezawa ², Xujun Liu ³ and Peihong Cong ³

¹ Graduate School of Science and Engineering, Kansai University, Osaka 564-8680, Japan; k915083@kansai-u.ac.jp

² Faculty of Engineering Science, Kansai University, Osaka 564-8680, Japan; hrstani@kansai-u.ac.jp (H.T.); s-kawada@kansai-u.ac.jp (S.K.); skoga@kansai-u.ac.jp (S.K.)

³ State Key Laboratory of Molecular Engineering of Polymers, Fudan University, Shanghai 200433, China; liuxujun@fudan.edu.cn (X.L.); congph@fudan.edu.cn (P.C.)

* Correspondence: r_lu@kansai-u.ac.jp; Tel.: +81-6-6368-0781

Abstract: Tribofilms, resulting from tribochemical reactions involving lubricants, additives, and metal surfaces, are pivotal in reducing friction, preventing adhesion, and minimizing wear. This study investigates the tribological characteristics of textured surfaces in boundary lubrication, emphasizing the impact of surface texturing on tribofilm formation. Untextured surfaces manifest high friction coefficients and low wear owing to the development of thick tribofilms. However, debris accumulation impedes further tribochemical reactions, necessitating more energy for sliding and resulting in higher friction coefficients. Additionally, molybdenum dialkyl dithiocarbamate-derived MoS₂ oxidation diminishes the expected lubrication effect. Textured surfaces exhibit lower friction coefficients and higher wear because the structure aids debris removal, promoting the formation of thinner tribofilms. Despite increased wear from solid-to-solid contact, textured surfaces facilitate an early fluid lubrication transition and enhance cavitation capacity, leading to reduced friction coefficients. We also consider the impact of sliding direction angles on friction coefficients, revealing that lower angles parallel to the grooves heighten friction, whereas higher angles enhance cavitation capacity. Unexpectedly, a 90° sliding direction angle increases the friction coefficients, attributed to MoS₂ distribution in the tribofilms. These results provide crucial insights for optimizing lubrication strategies and enhancing wear resistance in boundary lubrication scenarios.

Keywords: surface texture; friction reduction; tribofilm; zinc dialkyl dithiophosphate; molybdenum dialkyl dithiocarbamate



Citation: Li, Q.; Lu, R.; Tani, H.; Kawada, S.; Koganezawa, S.; Liu, X.; Cong, P. Tribofilm Formation and Friction Reduction Performance on Laser-Textured Surface with Micro-Grooved Structures. *Lubricants* **2024**, *12*, 91. <https://doi.org/10.3390/lubricants12030091>

Received: 13 February 2024

Revised: 9 March 2024

Accepted: 12 March 2024

Published: 13 March 2024



Copyright: © 2024 by the authors. Licensee MDPI, Basel, Switzerland. This article is an open access article distributed under the terms and conditions of the Creative Commons Attribution (CC BY) license (<https://creativecommons.org/licenses/by/4.0/>).

1. Introduction

Friction and wear are the primary concerns for moving parts and contact surfaces in mechanical operations. Approximately 23% of the global energy consumption is ascribed to frictional contacts [1]. Thus, reducing friction and minimizing wear are imperative for enhancing the efficiency, dependability, and longevity of mechanical components.

In the preceding two decades, surface texturing has emerged as a viable strategy for significantly enhancing the tribological design and application of mechanical components [2–7]. Surface texturing involves altering the surface topography to generate a consistent micro-relief characterized by systematically distributed protrusions or indentations. Numerous shapes, including triangles, rectangles, circles, stars, hexagons, sine textures, and composite textures using combinations of these shapes, have been investigated [8–10]. The surface depressions serve several purposes: first, they effectively reduce friction by capturing and removing wear particles from the surface [11,12]; second, they function as reservoirs for lubricant, providing secondary lubrication for the contacting surfaces and prolonging the lubricant's residence time [13–15]; third, the surface texture

can function as a microfluidic dynamic bearing between two parallel surfaces, generating hydrodynamic pressure by influencing cavitation and resulting in a reduced friction coefficient [16–20].

An alternative approach involves the development of effective tribofilms on contact surfaces [21–23]. Generally, tribofilms originate through chemical reactions occurring between additives and contacting surfaces under boundary lubrication conditions. In engine oils, zinc dialkyl dithiophosphate (ZDDP) is often added as an antiwear additive, and molybdenum dialkyl dithiocarbamate (MoDTC) is commonly used as a friction modifier. MoDTC typically exhibits a low friction coefficient, attributed to the formation of tribofilms containing MoS₂ [24,25]. ZDDP-induced tribofilms exhibit rough, patched-like features composed of pyrophosphate or orthophosphate glasses within the bulk, featuring an external nanoscale stratum of zinc polyphosphates and a sulfur-enriched layer proximate to the metal surface, protecting the surface from wear [26,27]. Tribofilms formed by the addition of ZDDP+MoDTC on sliding steel surfaces exhibit a dual-phase composition, encompassing Zn/Mo phosphate glass and a carbon-abundant amorphous phase containing MoS₂ sheets integrated within the phosphate glass. The synergy of ZDDP and MoDTC contributes to low friction and high anti-wear properties [28]. Initially formed at the contact region of sliding surfaces, the location and extent of tribofilm formation heavily depend on the surface morphology. ZDDP-derived tribofilm growth was elucidated by single-asperity sliding contacts, revealing an exponentially increasing growth rate with applied compressive stress or temperature, consistent with a reaction rate model activated by both thermal influences and stress [29,30]. However, the majority of tribofilm studies have focused on non-textured surfaces. Investigating tribofilm properties on textured surfaces is intriguing because the compressive stress is expected to improve owing to the reduced contact area, potentially influencing tribofilm formation.

The primary objective of this investigation was to scrutinize the influence of surface texture on the tribological attributes of tribofilms formed by ZDDP and MoDTC. It is anticipated that the findings of this study will offer significant insights into the optimization of lubrication strategies and the enhancement of wear resistance in boundary lubrication scenarios, including, but not limited to, the lubrication of piston/cylinder contacts, crankshaft bearings, and conformal contact components in compressors.

In this study, employing femtosecond laser technology, we generated surface textures with a depth of 20 µm on AISI 52100 steel. Friction tests were conducted using a ball-on-disk friction tester to demonstrate the influence of these fabricated textures on friction. Finally, X-ray photoelectron spectroscopy (XPS) was employed to characterize the tribofilms, revealing the correlation between tribofilm formation and surface texture.

2. Materials and Methods

2.1. Samples

In the test, AISI 52100 steel disks measuring 20 mm in diameter and 5 mm in thickness were employed. The surface roughness was maintained at the roughness of Ra 0.047 µm and RMS 0.061 µm through mirror polishing. A subsequent laser process was conducted using a femtosecond laser with a wavelength of 343 nm. Figure 1a shows the top view, Figure 1b shows the 3D geometry, and Figure 1c shows the cross-sectional profile of the parallel grooves fabricated on the disk surfaces. As previously indicated, grooves can capture wear debris. Notably, the groove width must exceed the XPS analyzed area unless the analysis encompasses wear debris entrapped in the grooves. The XPS minimum analysis area was set at 20 µm in diameter; hence, the grooves were fabricated with dimensions of 20 µm in width, 40 µm in pitch, and 20 µm in depth.

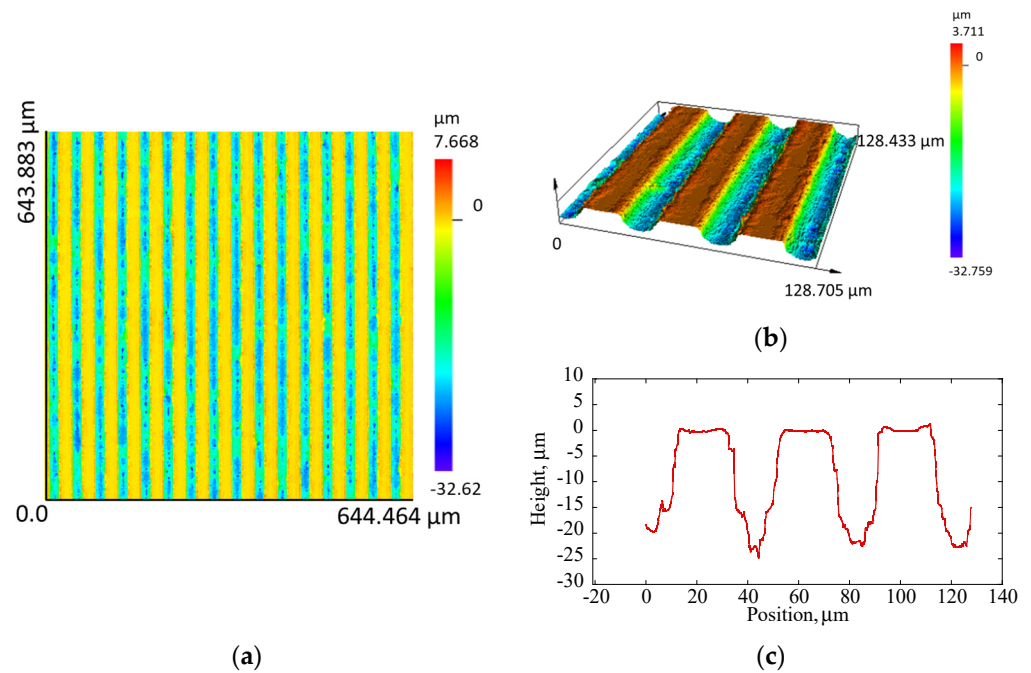


Figure 1. Surface texture fabricated on the AISI 52100 steel disk. (a) Top view; (b) 3D view; (c) cross-sectional profile.

The lubricant comprised two additives with surface-active properties: specifically, ZDDP at a concentration of 1 mass% and MoDTC at a concentration of 1 mass%. Synthetic oil polyalphaolefin (PAO6) was used as the base oil, which has a viscosity of $31 \text{ mm}^2 \cdot \text{s}^{-1}$ at 40°C and $5.8 \text{ mm}^2 \cdot \text{s}^{-1}$ at 100°C . The base oil and additives were supplied by MORESCO Corporation (Kobe, Japan).

2.2. Tribological Tests

A reciprocating ball-on-disk friction tester (Heidon-14DR, SHINTO Scientific Co., Ltd., Tokyo, Japan), as depicted in Figure 2, was employed for evaluating friction coefficients. The testing apparatus utilized a ball composed of AISI 52100 steel with a 6.35 mm diameter. A velocity of $10.0 \text{ mm} \cdot \text{s}^{-1}$ was imposed, and a uniform load of 5 N was applied for all friction tests. In this scenario, the maximum Hertzian contact stress reached 1.08 GPa under the ball-on-flat contact condition. While the friction tests were initially anticipated to encompass higher contact conditions, the experimental constraints were imposed by the load capacity limitations of the friction tester. The sliding stroke was fixed at 5.0 mm, and each test session extended for a duration of 1 h.

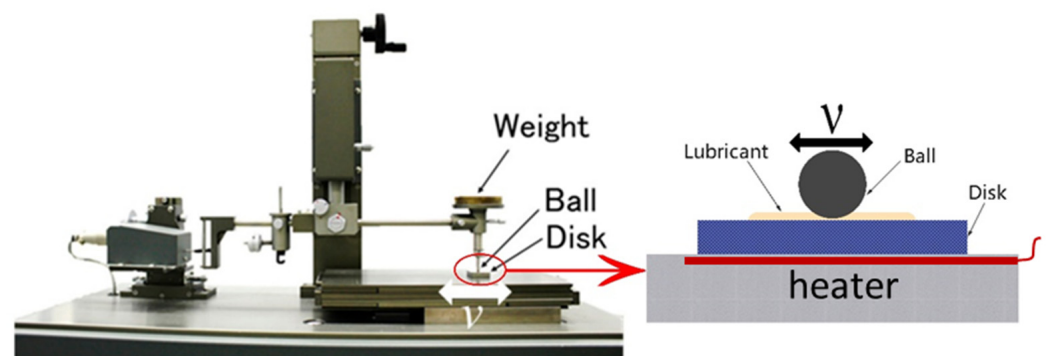


Figure 2. Image and illustration of the reciprocating friction tester.

Preceding each trial, the ball and disk underwent cleaning with acetone and hexane to eliminate surface contaminants. Subsequently, upon mounting the disk onto the friction tester, an oil volume of 3 mL was applied to the disk surface, initiating the formation of a consistent and stable oil film. Because tribofilms derived from ZDDP and MoDTC are generally formed between 60 and 80 °C, all the tribological tests were carried out under elevated temperatures, with the lubricant oils precisely regulated at 70 ± 2 °C using a built-in heater situated underneath the disk. The relative humidity was 40~60%. Each test condition was replicated at least three times.

The friction tests were conducted at the sliding direction angles of 0°, 15°, 30°, 45°, 60°, 75°, and 90° relative to the parallel grooves of the surface texture, as shown in Figure 3.

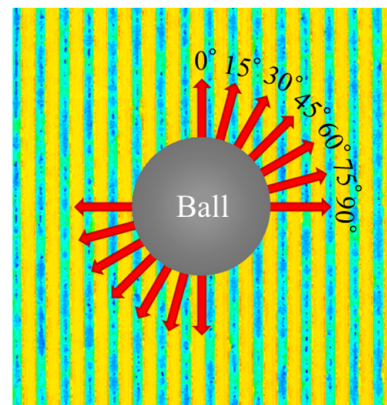


Figure 3. The sliding directions employed during friction tests.

2.3. Characterization

Following the completion of the friction tests, the specimens underwent a hexane rinse to eliminate any surplus lubricant. Subsequently, the wear tracks on both the disks and balls were examined using a confocal laser scanning microscope (OLS5000, Olympus, Tokyo, Japan).

For the examination of the tribofilms developed on friction surfaces, XPS analysis was conducted utilizing a PHI X-tool scanning X-ray microprobe (ULVAC-PHI, Kanagawa, Japan). The excitation of photoelectrons was achieved through monochromated Al-K α at 5 W and 15 kV. Scanning X-ray images facilitated the identification of convex features on the textured surface, aiding in the distinction between wear tracks and external areas. Ar⁺ sputtering was used for XPS depth profiling to investigate the thickness and elemental composition of the tribofilms. The sputtering rate was $9.61 \text{ nm} \cdot \text{min}^{-1}$, and the calibrated depth for the comprehensive analysis, utilizing a SiO₂ film, was 200 nm. Spectra were acquired with a beam diameter of 20 μm , a pass energy of 112 eV, and a step size of 0.1 eV. The collection was performed at a take-off angle of 45°. To calibrate the binding energies of the spectra, alignment was carried out based on the maximum C 1 s peak at 284.8 eV.

3. Results and Discussion

3.1. Effect of Surface Texture on the Friction Coefficient

Figure 4a–h depicts the evolution of friction coefficients over time for both the untextured surface and textured surfaces with varying sliding directions. Initially, the untextured surface exhibited a declining trend in the friction coefficient, followed by a rapid increase, stabilizing at a higher value of approximately 0.118. In contrast, the textured surfaces displayed a reduction in the friction coefficient during the running-in process, eventually reaching a stable state. Furthermore, the friction coefficient for textured surfaces decreased as the sliding angle increased. These findings indicate that the impact of surface texturing on friction was significantly influenced by the sliding direction.

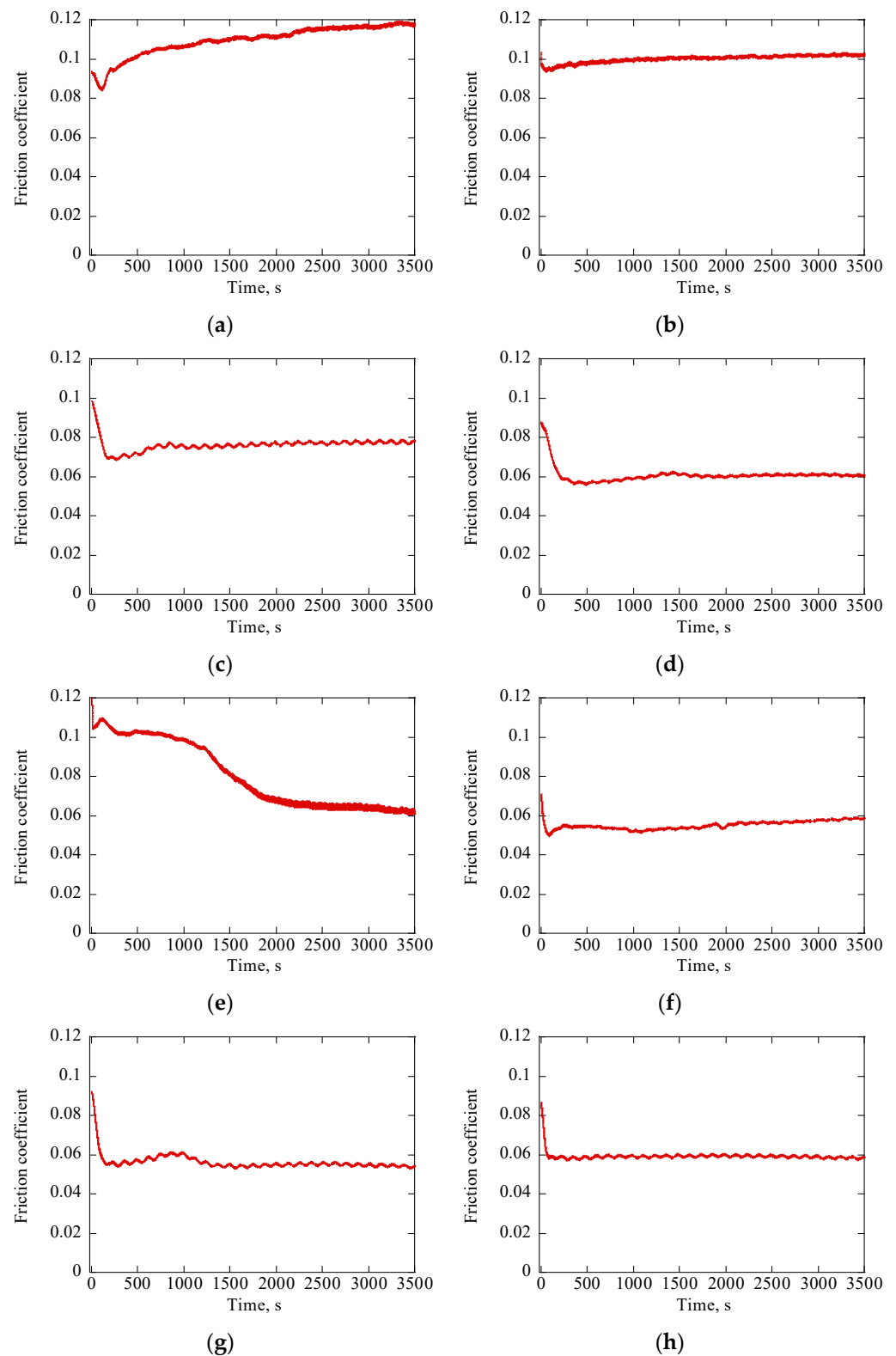


Figure 4. Change in the friction coefficient over time. (a) Untextured surface; (b) 0° on the textured surface; (c) 15° on the textured surface; (d) 30° on the textured surface; (e) 45° on the textured surface; (f) 60° on the textured surface; (g) 75° on the textured surface; (h) 90° on textured surface.

The average steady-state friction coefficients derived from the curves presented in Figure 4 are summarized in Figure 5. The untextured surface exhibited the highest friction coefficient, registering at 0.116, and the friction coefficient only decreased to 0.107 for the

textured surface with a parallel sliding direction to the grooves (i.e., a sliding direction angle of 0°). An increase in the sliding direction angle to 15° resulted in a significantly lower friction coefficient of 0.067. As the sliding direction angle continued to increase, the friction coefficient gradually decreased, reaching a minimum friction coefficient of 0.054 at a sliding direction angle of 75° , marking a 53% reduction compared with the untextured surface. Despite a relatively higher friction coefficient of 0.063 at a sliding direction angle of 90° , the surface texture exerts a favorable overall influence on the friction coefficient.

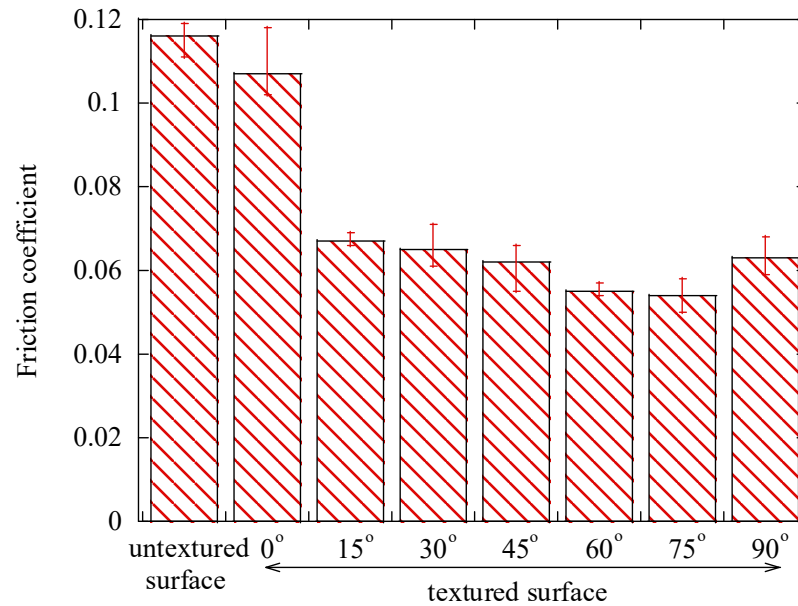


Figure 5. Effect of surface textures and sliding direction on the average friction coefficient.

3.2. Effect of Surface Texture on Wear

Figure 6 presents 2D images, surface profile curves, and 3D representations of the worn surfaces on the disks. Wear scars are observable on these surfaces, with the untextured surface exhibiting a wear scar width of $358.2 \mu\text{m}$, surpassing those on the textured surfaces. However, the surface profile indicates minimal wear occurring at the center of the untextured rubbing surface, as most of it is covered with a tribofilm up to $1 \mu\text{m}$ thick. This thick tribofilm acts as a cushion, augmenting the contact area and friction [31]. Conversely, on the textured surfaces, the grooves display wear, and no discernible tribofilm is formed on the rubbing surface. Additionally, the groove depth beneath the rubbing surface diminishes, signifying the accumulation of wear debris in the grooves.

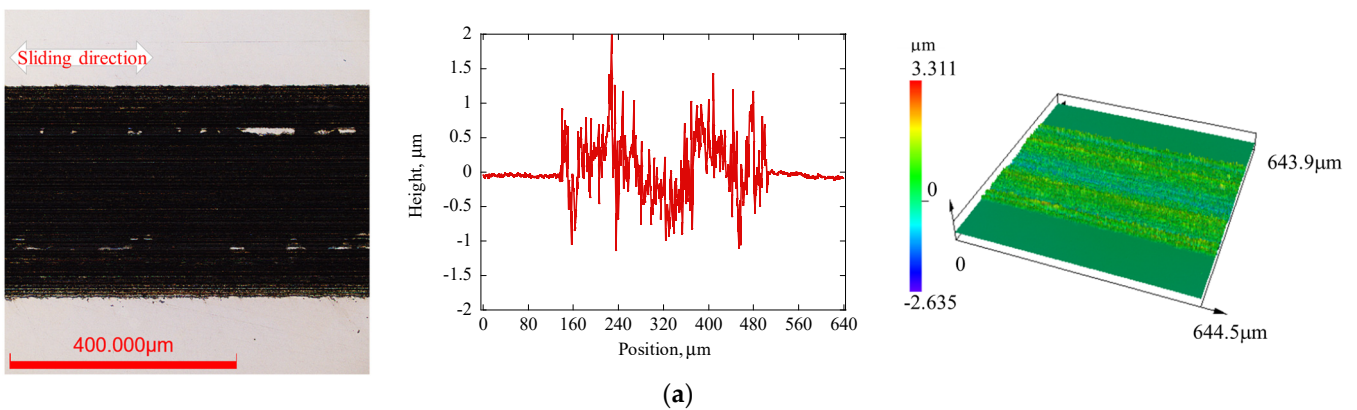


Figure 6. Cont.

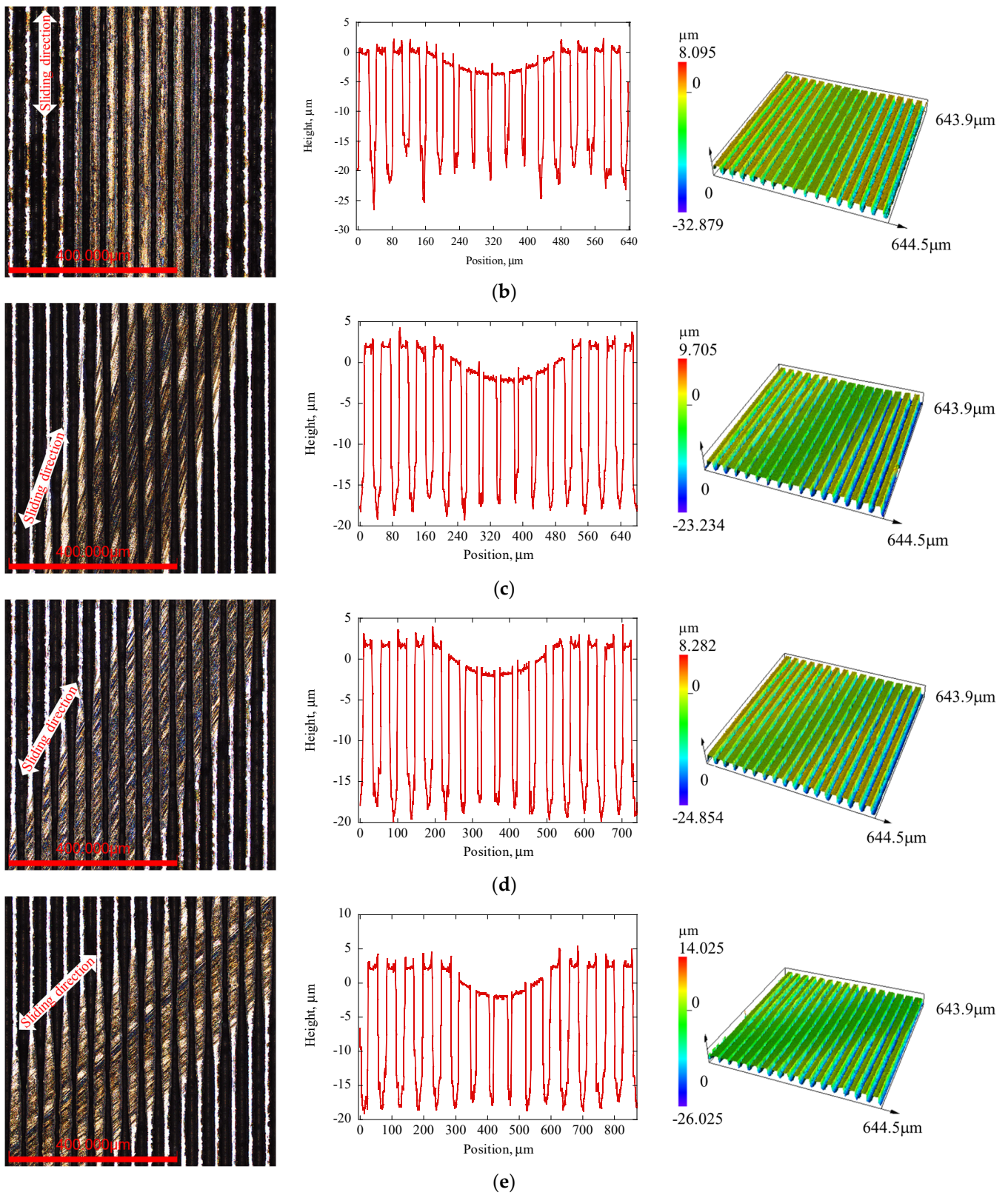


Figure 6. Cont.

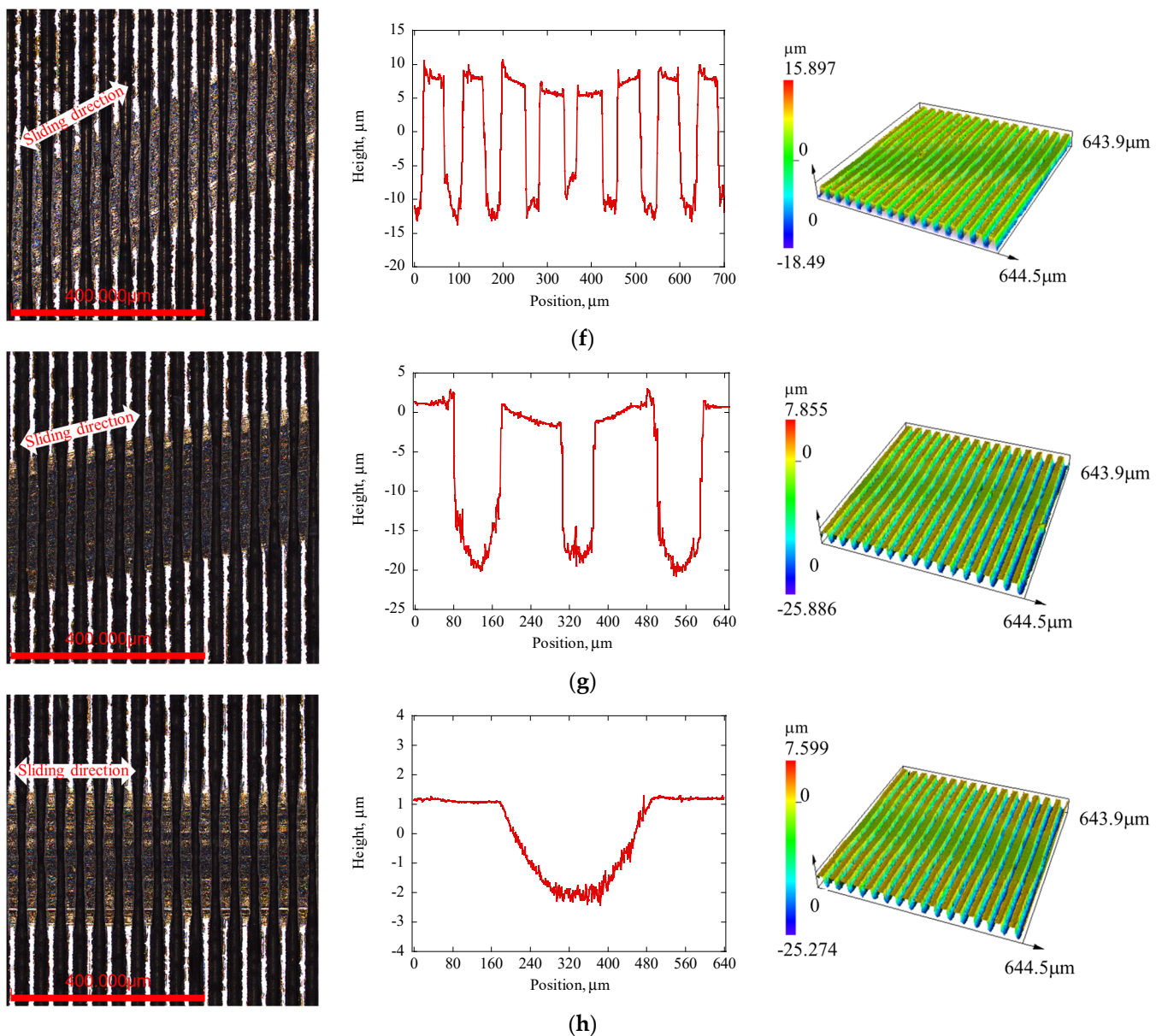


Figure 6. 2D images, surface profile curves, and 3D images of worn disk surfaces. (a) Untextured surface; (b) 0° on the textured surface; (c) 15° on the textured surface; (d) 30° on the textured surface; (e) 45° on the textured surface; (f) 60° on the textured surface; (g) 75° on the textured surface; (h) 90° on the textured surface. Note that the surface profile was measured perpendicular to the sliding direction.

Figure 7 shows the morphologies of friction tracks and surface profiles on the steel balls. The y direction denotes the sliding orientation. Evident wear manifested on the ball surface when the friction test was carried out on the untextured disk surface. The wear scar exhibited an almost circular morphology, with a diameter of approximately $355 \mu\text{m}$, aligning seamlessly with the width of the wear scar on the disk surface, as depicted in Figure 6a. Additionally, discernible tribofilms were found on the worn surface, indicating their formation on both sides of the contact interfaces. Conversely, when the friction test was carried out on the textured surface and the sliding direction was parallel to the grooves (i.e., the sliding direction angle of 0°), a friction track on the spherical surface assumed a rounded rectangular form. In this scenario, the spherical shape of the surface profiles implied negligible wear, while the roughness of the surface profiles within the

contact region signified the development of tribofilms. Surface texturing on disks helped to reduce the wear of counterfaces. Furthermore, tribofilms were evident beyond the confines of the rounded rectangular area, aligning with the grooves on the disk. This recurrent phenomenon persisted on the textured surface, irrespective of the sliding directions. It is known that Hertz theory finds application in ball-on-disk experiments when the disk surface is flat, and plastic deformation is absent. Consequently, wear scars on the balls adopt an almost circular configuration when sliding on untextured disk surfaces. However, on textured surfaces, the pressure distribution along the x direction became uniform, resulting in a rounded rectangular shape within the contact zone [32].

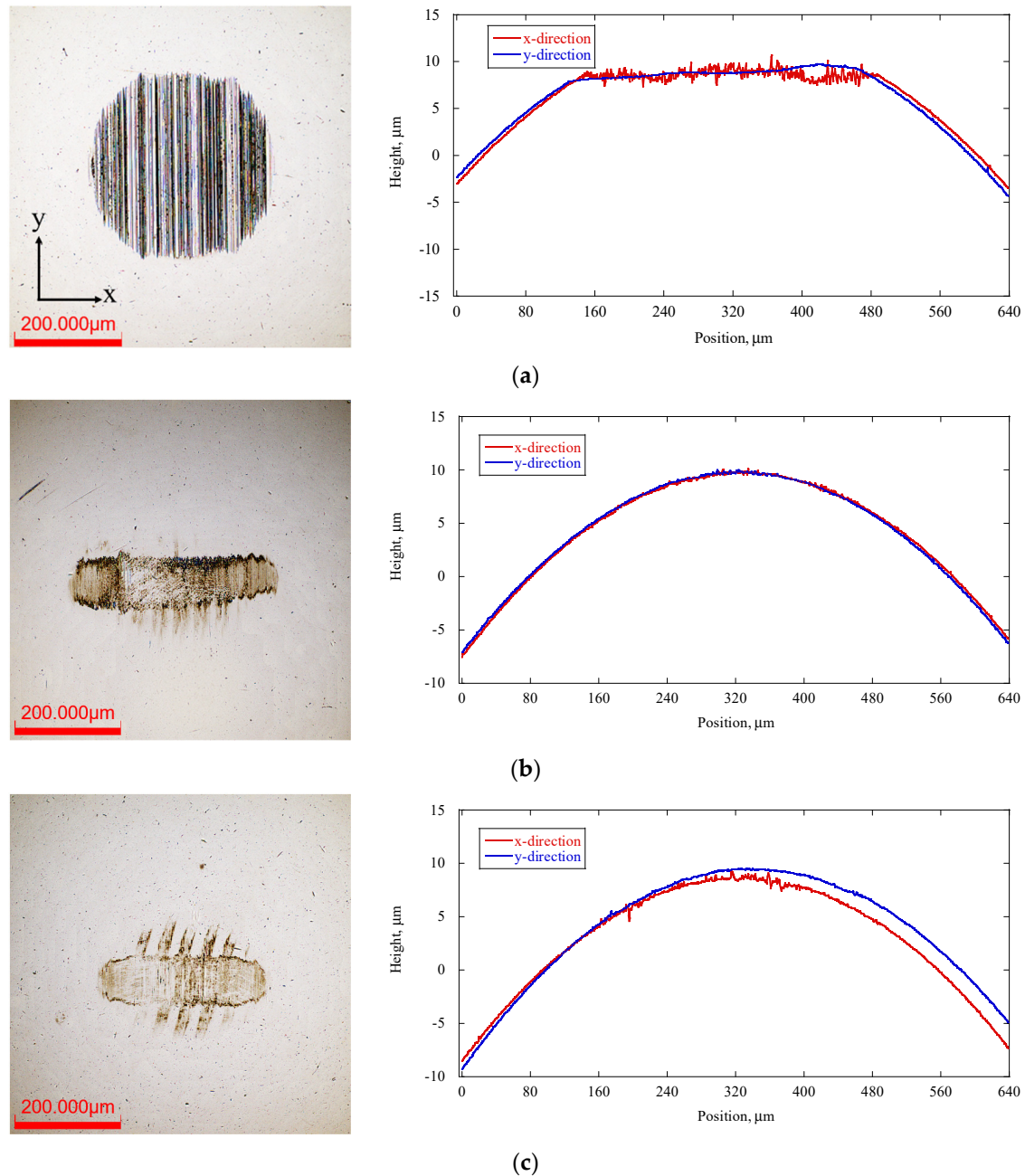
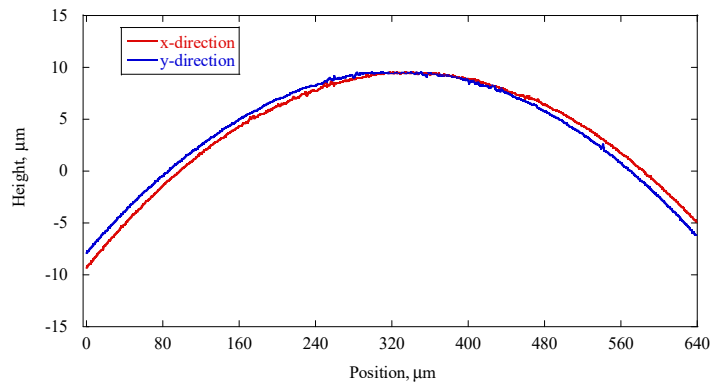
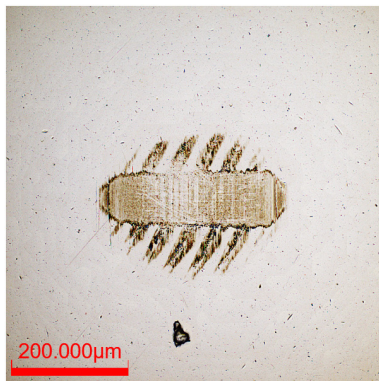
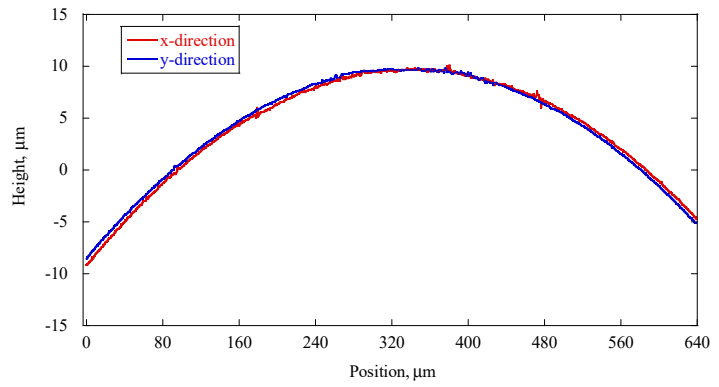
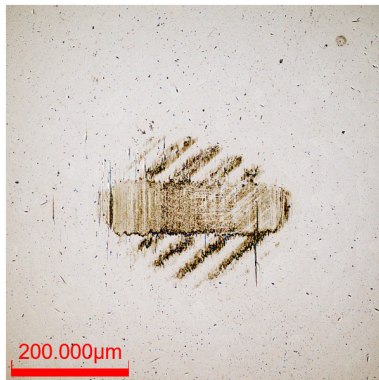


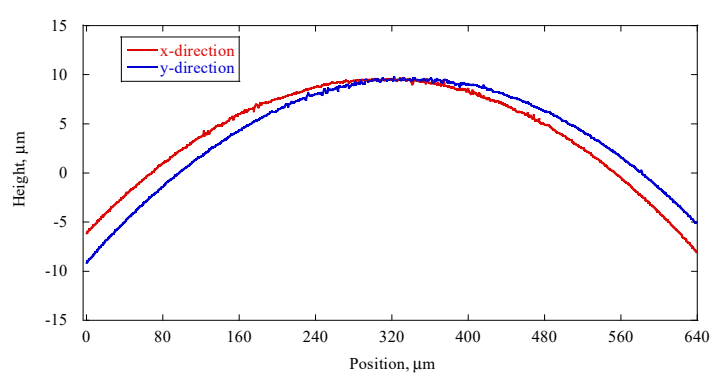
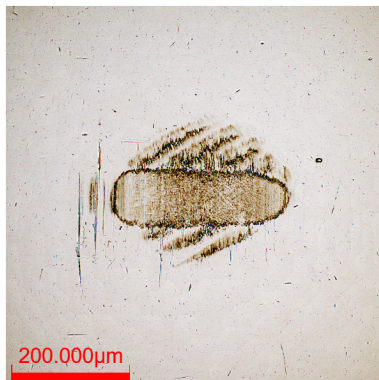
Figure 7. Cont.



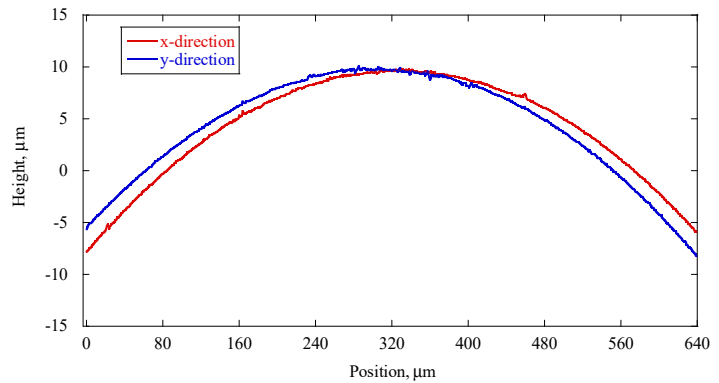
(d)



(e)



(f)



(g)

Figure 7. Cont.

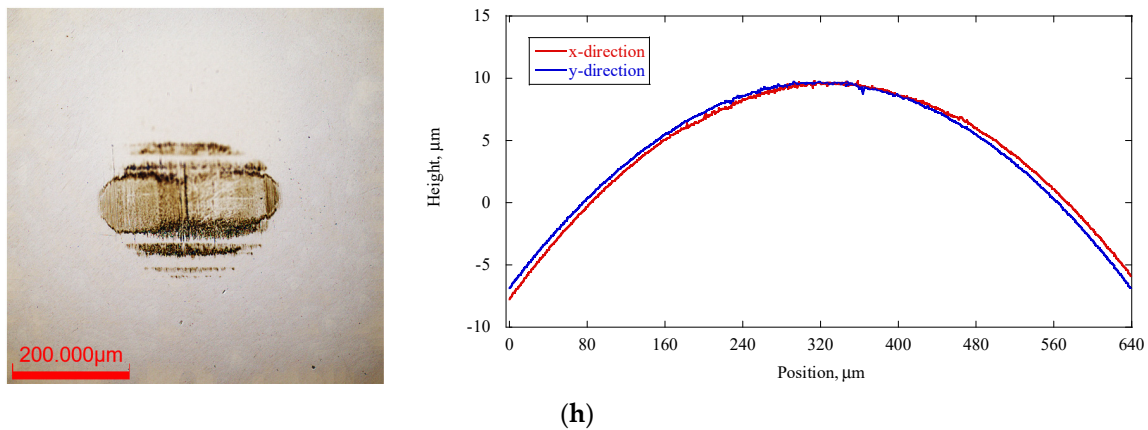


Figure 7. Wear morphologies and surface profiles on the balls. (a) Untextured surface; (b) 0° on the textured surface; (c) 15° on the textured surface; (d) 30° on the textured surface; (e) 45° on the textured surface; (f) 60° on the textured surface; (g) 75° on the textured surface; (h) 90° on textured surface.

Despite the persistent manifestation of contact surfaces in a rounded rectangular configuration, the contact area exhibited variability upon alteration of the sliding direction. For a quantitative assessment of this discrepancy, the parameter L_x denoted the width of the friction scar in the x direction, while L_y represented the width in the y direction. The ratio L_x/L_y approximated 4.5 when the sliding direction paralleled the grooves. As the sliding angle increased, the L_x/L_y ratio decreased to 3.9 at a sliding direction angle of 15° on the textured surface, 4.0 at 30° , 4.0 at 45° , 3.5 at 60° , 3.3 at 75° , and 3.3 at 90° . The diminishing L_x/L_y ratio was ascribed to the augmentation of the contact region between a designated groove and the sphere surface, concomitant with the elevation of the sliding direction angle.

Given the minimal wear observed on the balls during their movement across textured disk surfaces, it can be inferred that wear rate approached zero. Consequently, Figure 8 exclusively provides a summary of the wear scar widths and wear rates derived from the disks. Typically, the introduction of texturing is expected to entrap wear debris, thereby mitigating plowing and preventing abrasion [11,12]. However, in this study, the wear rate increased on textured surfaces despite the entrapment of wear debris. Tribofilms are commonly implicated in a dynamic evolution of formation and wear occurring amid friction [29,33]. On textured surfaces, the grooves facilitate the removal of debris particles from the contact surface, expediting the tribochemical reaction and consequently increasing wear. In contrast, on the untextured surface, the debris particles from the tribofilm remain, unable to escape the contact area, accumulating on the surface and providing protection against wear. Additionally, the heightened contact pressure resulting from a reduced contact area is a significant contributing factor.

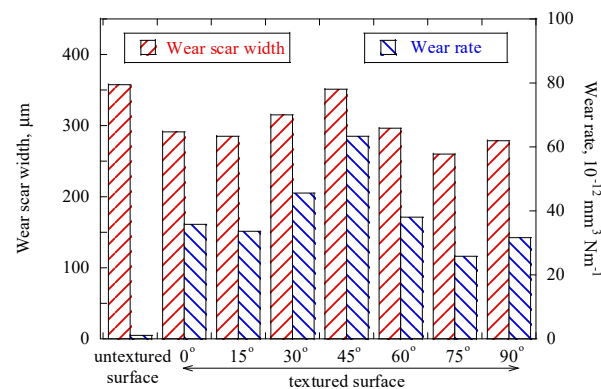


Figure 8. Effect of surface texture and sliding direction on the wear scar width and wear rate of disks.

3.3. Effect of Surface Texture on the Chemical Structure of the Tribofilm

The XPS analysis of tribofilms on disk surfaces was performed to elucidate the impact of surface textures on the chemical composition of these tribofilms. Figure 9 delineates the atomic percentages of C, O, P, S, Fe, Zn, and Mo within the tribofilms. In the initial 1.5 nm of sputtering on the untextured surface, the Fe proportion remains minimal (<10%), whereas the C proportion is high (>35%), signifying that the top layer of the film is predominantly composed of oligomers generated by the base oil. The proportions of P, S, Zn, and Mo remain relatively constant up to 200 nm, whereas the Fe proportion increases to approximately 73%. These findings indicate the formation of a tribofilm exceeding 200 nm on the untextured surface, as observed in Figure 6a.

On the textured surface, when the friction occurs parallel to the grooves (i.e., a sliding direction angle of 0°), the Fe proportion experiences a rapid increase with sputtering depth, leveling off at approximately 120 nm. This suggests that iron from the steel substrate was predominantly detected, with a tribofilm thickness of 120 nm. Additionally, the proportions of S and Mo remain above 5% until the sputtering depth reaches 20 nm, gradually decreasing and becoming negligible above 70 nm. This suggests an accumulation of debris derived from MoDTC in the top layer. Similar patterns are observed on the textured surfaces with different sliding directions, as depicted in Figure 9c–h.

From the XPS depth profile data, the predominant S 2p peak at 161.28 eV signifies the presence of sulfur, primarily in the form of metal sulfide. Simultaneously, the P 2p peak at 133.3 eV corresponds to metal phosphate [34]. In the Zn 2p spectrum, the primary peak at 1022.2 eV signifies the development of zinc sulfide [34,35]. The chemical states of S, P, and Zn on textured surfaces do not exhibit any discernible differences from those on the untextured surface.

In Figure 10, XPS Mo 3d spectra are presented with respect to sputtering depth. On the untextured surface, the Mo 3d spectra exhibit a prominent peak at 232.5 eV, suggesting the formation of molybdenum oxide [36]. Beyond a sputtering depth of 50 nm, a peak emerges at 229.1 eV, indicating the formation of molybdenum disulfide [36]. MoDTC typically exhibits a low friction coefficient, attributed to the development of a tribofilm containing MoS_2 . However, in this case, MoS_2 is identified beneath the top layer, rendering it ineffective in providing lubrication to the contact surfaces, leading to a relatively high friction coefficient. Note that the top layer of the tribofilm is exposed to air, leading to the oxidation of MoS_2 during the friction process [37].

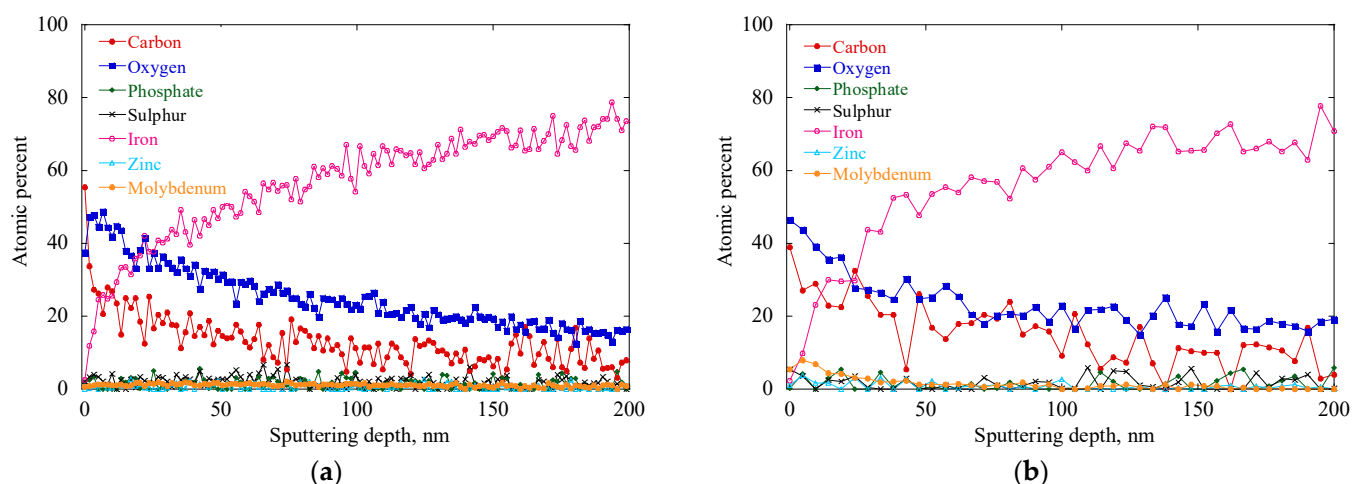


Figure 9. Cont.

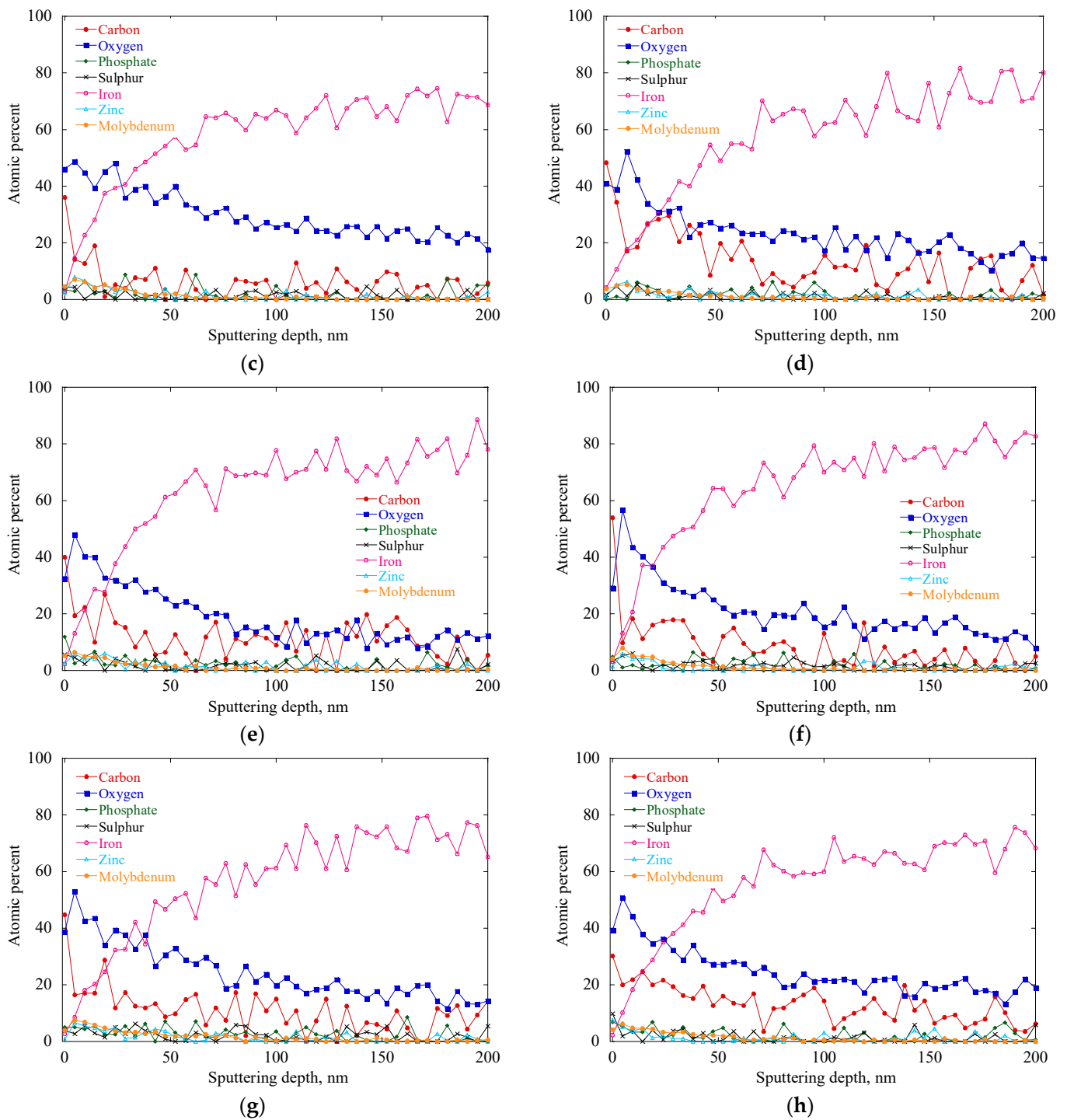


Figure 9. Atomic percent of different elements in the tribofilms as a function of sputtering depth. (a) Untextured surface; (b) 0° on the textured surface; (c) 15° on the textured surface; (d) 30° on the textured surface; (e) 45° on the textured surface; (f) 60° on the textured surface; (g) 75° on the textured surface; (h) 90° on the textured surface.

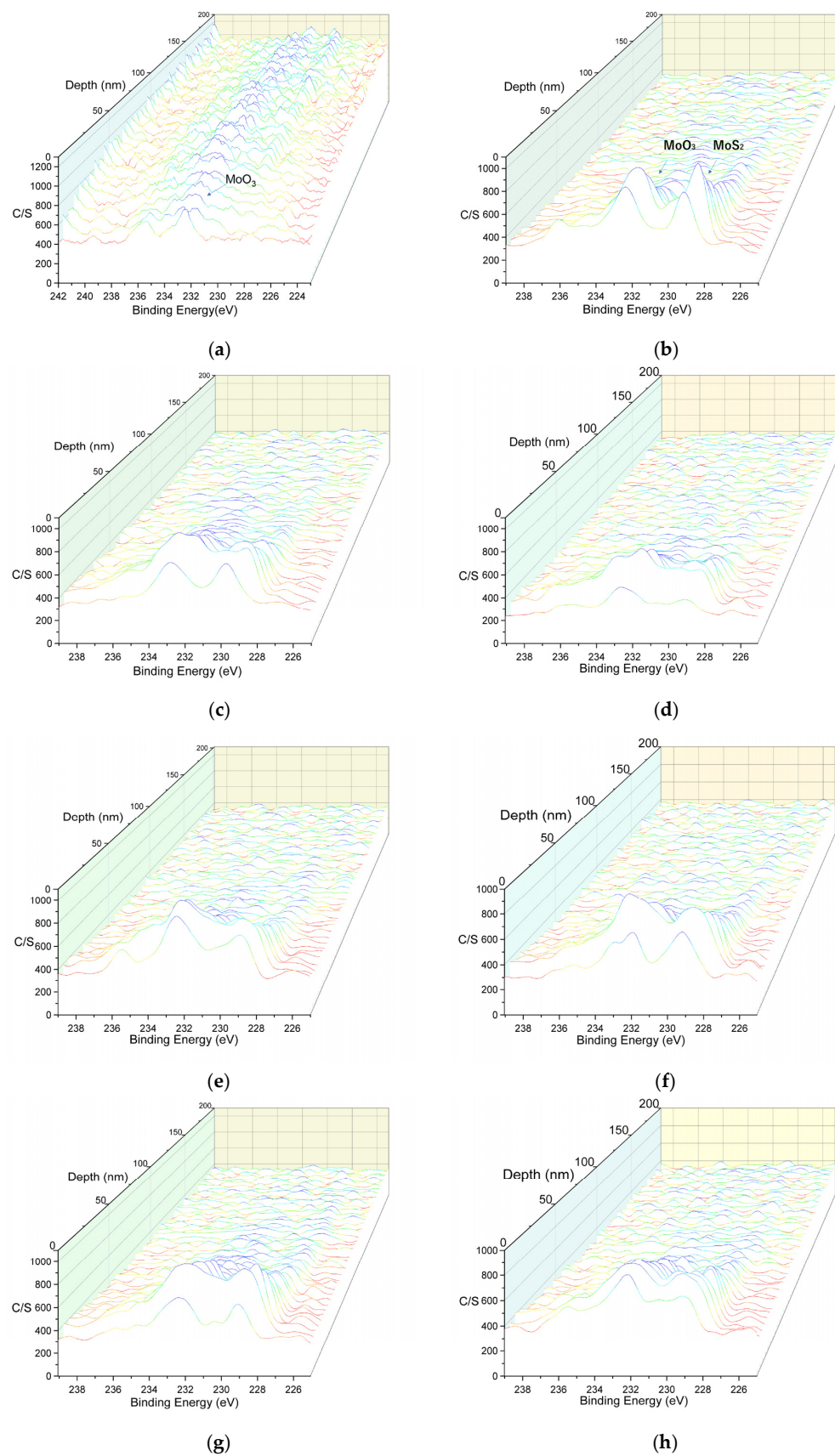


Figure 10. XPS Mo 3d spectra. (a) Untextured surface; (b) 0° on the textured surface; (c) 15° on the textured surface; (d) 30° on the textured surface; (e) 45° on the textured surface; (f) 60° on the textured surface; (g) 75° on the textured surface; (h) 90° on the textured surface.

On the textured surfaces, the consistent presence of peaks at 229.1 eV suggests the presence of MoS₂ within the outer layer of the tribofilm. Despite the unavoidable oxidation of MoS₂ during the friction process, both oxidized and unoxidized tribofilms can be eradicated by friction because the debris is entrapped within the grooves. The removal of the tribofilm from the contact surface prompts the generation of a new tribofilm through tribochemical reactions between additives and metal surfaces. Consequently, MoS₂ is consistently detected on the surface. Conversely, on the untextured surface, the debris cannot easily escape from the contact surfaces. The debris particles amalgamate, forming thicker films on the surface, hindering subsequent tribochemical reactions between additives and metal surfaces.

3.4. Discussion

Our observations validate that the non-textured surface displays an elevated friction coefficient and reduced wear, attributed to the presence of a substantial tribofilm. The initial interaction between the ball and the disk induces a heightened friction coefficient due to the inherent surface roughness. This condition persists until the surface gradually becomes smooth, leading to a decreasing trend in the friction coefficient. However, upon the removal of the metal surface layer, a newly exposed, highly active surface interacts with the lubricant and additives, triggering subsequent tribochemical reactions and the formation of tribofilms. During the friction process, debris from the tribofilm accumulates on the contact surface. On the untextured surface, depicted in Figure 11a, these debris particles cannot easily escape from the contact surfaces, resulting in their coalescence and the formation of thicker films on the surface. This impedes further tribochemical reactions between additives and metal surfaces. Concurrently, solid-to-solid contact is minimized, reducing wear. Given that the thick tribofilms typically comprise oligomers, more energy is required for the ball to slide on the tribofilm, leading to a higher friction coefficient. Additionally, the oxidation of MoS₂ derived from MoDTC diminishes the lubrication effect of MoDTC.

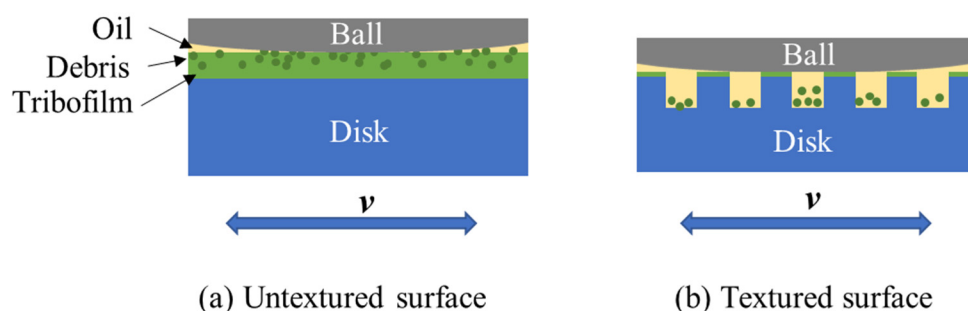


Figure 11. Illustration comparing tribofilm formation on the (a) untextured and (b) textured surfaces.

On textured surfaces, the friction-induced removal of debris from the tribofilm is facilitated by the grooves, as depicted in Figure 11b. This mechanism reduces the coalescence of debris on the top surface, resulting in the formation of thinner tribofilms. Traditionally, tribofilms are considered to undergo a dynamic evolution of formation and wear occurring amid friction. In this dynamic process, avoiding solid contact is not recommended because it leads to increased wear. In this particular scenario, the surface texture exhibits a detrimental effect on the wear resistance.

In contrast, the textures expedite the swift transition to fluid lubrication. Moreover, the grooves serve as an array of micro-bearings, augmenting cavitation capability. Cavitation enhances the separation between contacting surfaces, ensuring a continuous provision of lubricant oil by intensifying hydrodynamic lift [38,39]. Consequently, the friction coefficient on textured surfaces is diminished in comparison to untextured surfaces.

Moreover, the friction coefficient decreases with an increase in the sliding direction angle, as illustrated in Figure 5. A lower sliding direction angle approaches a direction

almost parallel to the grooves, whereas a higher sliding direction angle approaches a near-perpendicular orientation to the grooves. As suggested in Figure 12, cavitation capacity becomes negligible at a sliding direction angle of 0°, resulting in a higher friction coefficient. As the sliding direction angle increases, cavitation capacity proportionally increases, and the maximum cavitation capacity is anticipated when the sliding direction is set to 90°. Most of the observed friction coefficients are consistent with this assumption. However, the friction coefficient at a sliding direction angle of 90° increased compared with that at 75°, suggesting the presence of other contributing factors. Figure 13 depicts the MoS₂ thickness in the tribofilms according to the XPS depth analysis, revealing an inverse correlation between the depth of MoS₂ in the tribofilm and the sliding direction angles above 15°. In addition to cavitation capacity, the distribution of MoS₂ significantly affects the friction coefficient.

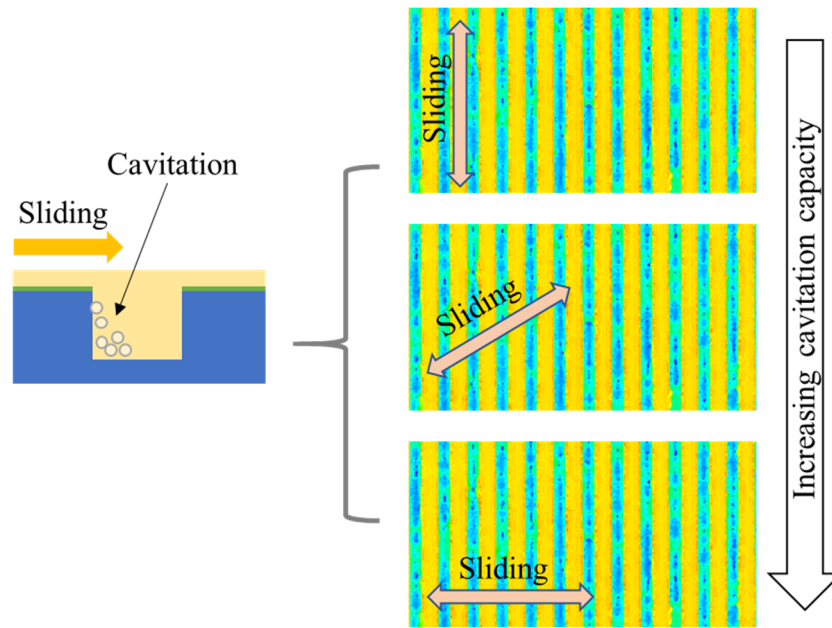


Figure 12. Schematic of cavitation capacity on textured surfaces.

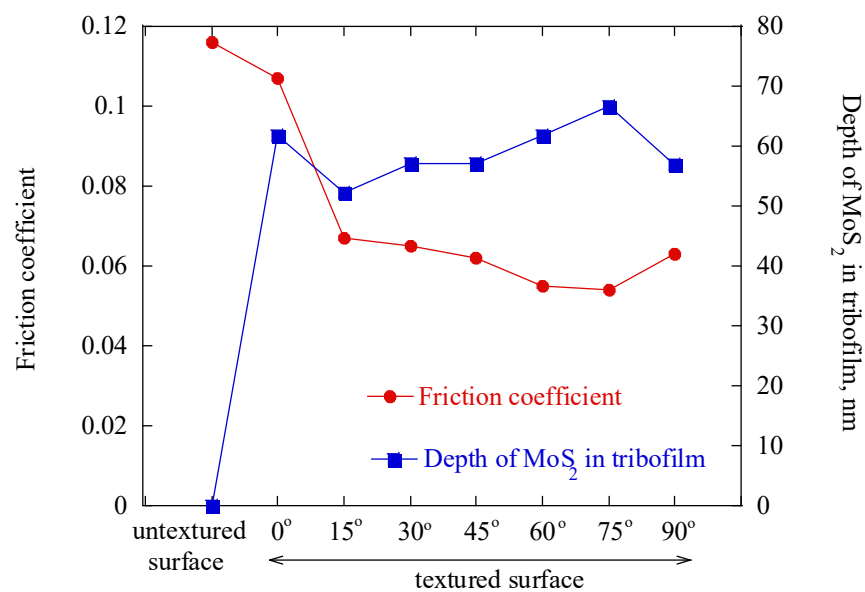


Figure 13. Correlation between the friction coefficient and the depth of MoS₂ in tribofilms formed on untextured and textured surfaces.

4. Conclusions

Tribofilms form through intricate tribochemical reactions involving lubricants, additives, and metal surfaces, playing a vital role in diminishing friction, preventing adhesion, and minimizing wear. The present work focuses on the tribological characteristics of textured surfaces in boundary lubrication conditions, emphasizing the impact of surface texturing on tribofilm formation and behavior. The primary findings are outlined below.

The untextured surface exhibits a high friction coefficient and low wear due to the formation of thick tribofilms. Debris tends to accumulate, forming thicker tribofilms and impeding further tribochemical reactions, ultimately reducing wear. However, more energy is needed to slide on the tribofilm, resulting in a higher friction coefficient. Furthermore, the oxidation of MoS₂ derived from MoDTC compromised the lubricating effectiveness of MoDTC.

In contrast, textured surfaces display lower friction coefficients and higher wear. The textured structure aids in debris removal, mitigating coalescence and promoting the formation of thinner tribofilms. Although solid-to-solid contact increases wear, textured surfaces facilitate early fluid lubrication transition and enhance cavitation capacity, contributing to reduced friction and energy consumption in mechanical operations.

Evident wear was discerned on the surface of the ball during sliding on the non-textured surface, manifesting as a circular wear scar. In contrast, no discernible wear was observed on the ball surface during sliding on the textured surface, where a friction track characterized by a rounded rectangular shape within the contact zone was identified. It can be inferred that textured surfaces offer potential advantages in minimizing wear on contacting surfaces.

The study also considers the impact of sliding direction angles on friction coefficients. Lower angles (i.e., sliding directions almost parallel to the grooves) increase friction, whereas higher angles (i.e., sliding directions almost perpendicular to grooves) enhance cavitation capacity. However, the friction coefficient at a 90° sliding direction angle exhibits an unexpected increase, attributed to factors other than cavitation capacity, such as the distribution of MoS₂ in the tribofilms.

Clarifying the intricate relationships among surface texturing, tribofilm formation, and sliding conditions provides valuable insights for optimizing lubrication strategies and improving wear resistance in boundary lubrication scenarios.

Author Contributions: Conceptualization, R.L.; methodology, R.L.; validation, Q.L. and R.L.; formal analysis, Q.L. and R.L.; investigation, R.L., Q.L., H.T., S.K. (Shohei Kawada), S.K. (Shinji Koganezawa), X.L. and P.C.; writing—original draft preparation, R.L. and Q.L.; writing—review and editing, R.L.; supervision, R.L.; project administration, X.L. and P.C.; funding acquisition, R.L., X.L., and P.C. All authors have read and agreed to the published version of the manuscript.

Funding: This research was partially funded by a Senior Visiting Scholarship from Fudan University, grant number 2024FGJ03.

Data Availability Statement: Data are contained within the article.

Conflicts of Interest: The authors declare no conflicts of interest.

References

1. Holmberg, K.; Erdemir, A. Influence of tribology on global energy consumption, costs and emissions. *Friction* **2017**, *5*, 263–284. [[CrossRef](#)]
2. Ibatan, T.; Uddin, M.S.; Chowdhury, M.A.K. Recent development on surface texturing in enhancing tribological performance of bearing sliders. *Surf. Coat. Technol.* **2015**, *272*, 102–120. [[CrossRef](#)]
3. Xi, Y.; Choi, C.; Chang, R.; Kaper, H.J.; Sharma, P.K. Tribology of pore-textured hard surfaces under physiological conditions: Effects of texture scales. *Langmuir* **2023**, *39*, 6657–6665. [[CrossRef](#)]
4. Xu, Y.; Zheng, Q.; Abuflaha, R.; Olson, D.; Furlong, O.; You, T.; Zhang, Q.; Hu, X.; Tysoe, W.T. Influence of dimple shape on tribofilm formation and tribological properties of textured surfaces under full and starved lubrication. *Tribol. Int.* **2019**, *136*, 267–275. [[CrossRef](#)]

5. Menezes, P.L.; Kishore; Kailas, S.V.; Lovell, M.R. Role of surface texture, roughness, and hardness on friction during unidirectional sliding. *Tribol. Lett.* **2011**, *41*, 1–15. [[CrossRef](#)]
6. Vishnoi, M.; Kumar, P.; Murtaza, Q. Surface texturing techniques to enhance tribological performance: A review. *Surf. Interfaces* **2021**, *27*, 101463. [[CrossRef](#)]
7. Ping, L.; Robert, J.K.W. Tribological performance of surface texturing in mechanical applications—A review. *Surf. Topogr. Metrol. Prop.* **2020**, *8*, 043001. [[CrossRef](#)]
8. Wu, Z.; Bao, H.; Xing, Y.; Liu, L. Tribological characteristics and advanced processing methods of textured surfaces: A review. *Int. J. Adv. Manuf. Technol.* **2021**, *114*, 1241–1277. [[CrossRef](#)]
9. Annadi, R.R.; Syed, I. Impact of multi-scaled surface textures on tribological performance of parallel sliding contact under lubricated condition. *Tribol. Int.* **2023**, *183*, 108415. [[CrossRef](#)]
10. Ali, S.; Kurniawan, R.; Chul, P.G.; Ko, T.J. Tribological properties of hierarchical micro-dimples produced on a cylindrical surface by dual-frequency texturing. *Friction* **2023**, *11*, 246–258. [[CrossRef](#)]
11. Zhao, X.; Zhang, Y. Tribological and dynamic performance analysis of rolling bearings with varied surface textures operating under lubricant contamination. *Wear* **2023**, *532–533*, 205109. [[CrossRef](#)]
12. Li, X.; Yue, W.; Huang, F.; Kang, J.; Zhu, L.; Tian, B. Tribological behaviour of textured titanium under abrasive wear. *Surf. Eng.* **2019**, *35*, 378–386. [[CrossRef](#)]
13. Ding, S.; Wei, H.; Yang, O.; Deng, L.; Mu, D. Tribological behaviors of laser textured surface under different lubrication conditions for rotary compressor. *Sci. Rep.* **2023**, *13*, 5378. [[CrossRef](#)]
14. Pettersson, U.; Jacobson, S. Influence of surface texture on boundary lubricated sliding contacts. *Tribol. Int.* **2003**, *36*, 857–864. [[CrossRef](#)]
15. Zhang, J.; Zhang, J.; Rosenkranz, A.; Zhao, X.; Song, Y. Surface textures fabricated by laser surface texturing and diamond cutting—Influence of texture depth on friction and wear. *Adv. Eng. Mater.* **2018**, *20*, 1700995. [[CrossRef](#)]
16. Huang, Q.; Shi, X.; Xue, Y.; Zhang, K.; Wu, C. Recent progress on surface texturing and solid lubricants in tribology: Designs, properties, and mechanisms. *Mater. Today Commun.* **2023**, *35*, 105854. [[CrossRef](#)]
17. Tang, W.; Zhou, Y.; Zhu, H.; Yang, H. The effect of surface texturing on reducing the friction and wear of steel under lubricated sliding contact. *Appl. Surf. Sci.* **2013**, *273*, 199–204. [[CrossRef](#)]
18. Yuan, S.; Lin, N.; Wang, W.; Zhang, H.; Liu, Z.; Yu, Y.; Zeng, Q.; Wu, Y. Correlation between surface textural parameter and tribological behaviour of four metal materials with laser surface texturing (LST). *Appl. Surf. Sci.* **2022**, *583*, 152410. [[CrossRef](#)]
19. Vlădescu, S.; Olver, A.V.; Pegg, I.G.; Reddyhoff, T. Combined friction and wear reduction in a reciprocating contact through laser surface texturing. *Wear* **2016**, *358–359*, 51–61. [[CrossRef](#)]
20. Gachot, C.; Rosenkranz, A.; Hsu, S.M.; Costa, H.L. A critical assessment of surface texturing for friction and wear improvement. *Wear* **2017**, *372–373*, 21–41. [[CrossRef](#)]
21. Parsaeian, P.; Ghanbarzadeh, A.; Van Eijk, M.C.P.; Nedelcu, I.; Neville, A.; Morina, A. A new insight into the interfacial mechanisms of the tribofilm formed by zinc dialkyl dithiophosphate. *Appl. Surf. Sci.* **2017**, *403*, 472–486. [[CrossRef](#)]
22. Ueda, M.; Kadiric, A.; Spikes, H. Influence of steel surface composition on ZDDP tribofilm growth using ion implantation. *Tribol. Lett.* **2021**, *69*, 62. [[CrossRef](#)]
23. Ueda, M.; Kadiric, A.; Spikes, H. On the crystallinity and durability of ZDDP tribofilm. *Tribol. Lett.* **2019**, *67*, 123. [[CrossRef](#)]
24. De Barros Bouchet, M.I.; Martin, J.M.; Le Mogne, T.; Bilas, P.; Vacher, B.; Yamada, Y. Mechanisms of MoS₂ formation by MoDTC in presence of ZnDTP: Effect of oxidative degradation. *Wear* **2005**, *258*, 1643–1650. [[CrossRef](#)]
25. Komaba, M.; Kondo, S.; Suzuki, A.; Kurihara, K.; Mori, S. The effect of temperature on lubrication property with MoDTC-containing lubricant. *Tribol. Online* **2018**, *13*, 275–281. [[CrossRef](#)]
26. Yin, Z.; Kasrai, M.; Fuller, M.; Bancroft, G.M.; Fyfe, K.; Tan, K.T. Application of soft X-ray absorption spectroscopy in chemical characterization of antiwear films generated by ZDDP Part I: The effects of physical parameters. *Wear* **1997**, *202*, 172–191. [[CrossRef](#)]
27. Martin, J.M.; Grossiord, C.; Le Mogne, T.; Bec, S.; Tonck, A. The two-layer structure of ZnDTP tribofilms: Part I: AES, XPS and XANES analyses. *Tribol. Int.* **2001**, *34*, 523–530. [[CrossRef](#)]
28. Morina, A.; Neville, A.; Priest, M.; Green, J.H. ZDDP and MoDTC interactions and their effect on tribological performance—Tribofilm characteristics and its evolution. *Tribol. Lett.* **2006**, *24*, 243–256. [[CrossRef](#)]
29. Gosvami, N.N.; Bares, J.A.; Mangolini, F.; Konicek, A.R.; Yablon, D.G.; Carpick, R.W. Mechanisms of antiwear tribofilm growth revealed in situ by single-asperity sliding contacts. *Science* **2015**, *348*, 102–106. [[CrossRef](#)]
30. Soni, J.; Gosvami, N.N. Recent advancements in understanding of growth and properties of antiwear tribofilms derived from zinc dialkyl dithiophosphate additives under nanoscale sliding contacts. *Langmuir* **2024**, *40*, 3301–3309. [[CrossRef](#)] [[PubMed](#)]
31. Dawczyk, J.; Morgan, N.; Russo, J.; Spikes, H. Film thickness and friction of ZDDP tribofilms. *Tribol. Lett.* **2019**, *67*, 34. [[CrossRef](#)]
32. Kucharski, S.; Mróz, Z. Identification of wear process parameters in reciprocating ball-on-disc tests. *Tribol. Int.* **2011**, *44*, 154–164. [[CrossRef](#)]
33. Lu, R.; Shiode, S.; Tani, H.; Tagawa, N.; Koganezawa, S. A study on the tribofilm growth and tribological properties of tribofilms formed from Zinc dialkyl dithiophosphate (ZDDP) and Molybdenum dialkyl dithiocarbamate (MoDTC). *Tribol. Online* **2018**, *13*, 157–165. [[CrossRef](#)]

34. Moulder, J.F.; Stickle, W.F.; Sobol, P.E.; Bomben, K.D. *Handbook of X-ray Photoelectron Spectroscopy*; Physical Electronics USA, Inc.: Chanhassen, MN, USA, 1995.
35. Hsu, C.-J.; Barrirero, J.; Merz, R.; Stratmann, A.; Aboufadel, H.; Jacobs, G.; Kopnarski, M.; Mücklich, F.; Gachot, C. Revealing the interface nature of ZDDP tribofilm by X-ray photoelectron spectroscopy and atom probe tomography. *Ind. Lubr. Tribol.* **2020**, *72*, 923–930. [[CrossRef](#)]
36. Lince, J.R.; Pluntze, A.M.; Jackson, S.A.; Radhakrishnan, G.; Adams, P.M. Tribochemistry of MoS₂ nanoparticle coatings. *Tribol. Lett.* **2014**, *53*, 543–554. [[CrossRef](#)]
37. Arif, T.; Yadav, S.; Colas, G.; Veer Singh, C.; Filleter, T. Understanding the independent and interdependent role of water and oxidation on the tribology of ultrathin molybdenum disulfide (MoS₂). *Adv. Mater. Interfaces.* **2019**, *6*, 1901246. [[CrossRef](#)]
38. Hsu, S.M.; Jing, Y.; Hua, D.; Zhang, H. Friction reduction using discrete surface textures: Principle and design. *J. Phys. D Appl. Phys.* **2014**, *47*, 335307. [[CrossRef](#)]
39. Mao, B.; Siddaiah, A.; Liao, Y.; Menezes, P.L. Laser surface texturing and related techniques for enhancing tribological performance of engineering materials: A review. *J. Manuf. Process.* **2020**, *53*, 153–173. [[CrossRef](#)]

Disclaimer/Publisher’s Note: The statements, opinions and data contained in all publications are solely those of the individual author(s) and contributor(s) and not of MDPI and/or the editor(s). MDPI and/or the editor(s) disclaim responsibility for any injury to people or property resulting from any ideas, methods, instructions or products referred to in the content.